Estimation of Tire Forces for Application to Vehicle Stability Control

Wanki Cho, Jangyeol Yoon, Seongjin Yim, Bongyeong Koo, and Kyongsu Yi

***Abstract*—Estimated tire forces can be used to implement unified-chassis-control (UCC) systems. This paper presents a scheme for longitudinal/lateral tire-force estimation. The longitudinal and lateral tire-force-estimation scheme has been designed, and this consists of the following five steps: vertical tire-force estimation, shaft torque estimation, longitudinal tire-force estimation based on a simplified wheel-dynamics model, lateral tire-force estimation based on a planar model, and the combined tire-force estimation. The combined tire-force-estimation scheme has been designed to compensate for the longitudinal/lateral tire-force estimator, which uses a random-walk Kalman filter. The proposed estimation scheme has been integrated into a UCC system. The performance of the UCC system, including the estimator, has been evaluated via computer simulations conducted using the vehicle dynamic software CARSIM, the ASM vehicle model, and the UCC system coded with Matlab/Simulink.**

***Index Terms*—Estimation, longitudinal/lateral tire-force estimator, random-walk Kalman filter, unified chassis control (UCC), vehicle lateral stability.**

NOMENCLATURE

a_x	Vehicle longitudinal acceleration.
a_y	Vehicle lateral acceleration.
c_i	Torque converter parameter $(i = 1, 2, \ldots, 6)$.
e_s	Height of the sprung mass from the roll axis $=$ 0.34 m.
g	Gravity acceleration.
h_r	Height of the roll center $= 0.56$ m.
h_a	Unsprung mass from the ground $= 0.379$ m.
l_f	Distance from the center of gravity (CG) to the front axle $= 1.07$ m.
l_r	Distance from the CG to the rear axle $= 1.78$ m.
m	Total mass of the vehicle $= 2450$ kg.
m_s	Sprung mass of the vehicle $= 2210$ kg.
m_u	Unsprung mass of the vehicle $= 120$ kg.
n_x	Longitudinal acceleration sensor noise.
n_y	Lateral acceleration sensor noise.
r	Original radius of the wheel $= 0.398$ m.
$r_{w,i}$	Effective radius of the wheel.
t	Tread (track width) $= 1.62$ m.
ω_p	Pump angular velocity.
ω_w	Wheel angular velocity.
ω_t	Turbine angular velocity.
C_f	Front tire cornering stiffness $= 7.2699e{+}004$ N/rad.
C_r	Rear tire cornering stiffness $= 5.8868e{+}004$ N/rad.
F_{rr}	Rolling resistance force.
F_x	Tire longitudinal force.
F_{SWF}	Static normal force of the front axle.
F_{SWR}	Static normal force of the rear axle.
$F_{x,FL}$	Longitudinal force of the front-left wheel.
$F_{x,FR}$	Longitudinal force of the front-right wheel.
$F_{x,RL}$	Longitudinal force of the rear-left wheel.
$F_{x,RR}$	Longitudinal force of the rear-right wheel.
$F_{y,FL}$	Lateral force of the front-left wheel.
$F_{y,FR}$	Lateral force of the front-right wheel.
$F_{y,RL}$	Lateral force of the rear-left wheel.
$F_{y,RR}$	Lateral force of the rear-right wheel.
$F_{z,FL}$	Vertical force of the front-left wheel.
$F_{z,FR}$	Vertical force of the front-right wheel.
$F_{z,RL}$	Vertical force of the rear-left wheel.
$F_{z,RR}$	Vertical force of the rear-right wheel.
I_{cr}	Turbine inertia $= 0.05623$ kg m^2.
I_w	Spin inertia for each wheel $= 1.1$ kg m^2.
I_z	Moment of inertia about the yaw axis $(\mathrm{o}) =$ 4331.6 kg m2.
K_{Bf}	Brake gain of the front wheel $= 350$ Nm/MPa.
K_{Br}	Brake gain of the rear wheel $= 300$ Nm/MPa.
K_s	Torsional spring constant.
K_t	Spring rate of the tire $= 250\,000$ N/m.
M_Z	Direct yaw moment.
P_{Bf}	Brake pressure of the front wheel.
P_{Br}	Brake pressure of the rear wheel.
R_d	Final drive gear ratio $= 0.3774$.
R_i	Ratio of each gear.
T_s	Shaft torque.
T_t	Turbine torque.
V_x	Vehicle longitudinal velocity, positive forward.
V_y	Vehicle lateral velocity, positive toward left.
W_{FA}	Longitudinal load transfer.
$W_{LTF,L}$	Lateral load transfer of the front-left wheel.
$W_{LTF,R}$	Lateral load transfer of the front-right wheel.
$W_{LTR,L}$	Lateral load transfer of the rear-left wheel.

Manuscript received April 1, 2009; revised August 7, 2009. First published October 13, 2009; current version published February 19, 2010. This work was supported in part by the Mando Corporation, by the BK21 program, SNU-IAMD, the Korea Research Foundation Grant funded by the Korean Government (MEST) under KRF-2009-200-D00003, and by the Institute of Advanced Machinery and Design, Seoul National University. The review of this paper was coordinated by Dr. S. Anwar.

W. Cho, J. Yoon, and K. Yi are with the School of Mechanical and Aerospace Engineering, Seoul National University, Seoul 151-744, Korea (e-mail: nawanki0@ snu.ac.kr; yun0714@snu.ac.kr; kyi@snu.ac.kr).

S. Yim is with the BK21 School of Creative Engineering Design of Next Generation Mechanical and Aerospace System, Seoul National University, Seoul 151-744, Korea (e-mail: thewait@naver.com).

B. Koo is with the Central R&D Center, Mando Corporation, Kyonggi-Do 446-901, Korea (e-mail: bgkoo@mando.com).

Color versions of one or more of the figures in this paper are available online at http://ieeexplore.ieee.org.

Digital Object Identifier 10.1109/TVT.2009.2034268

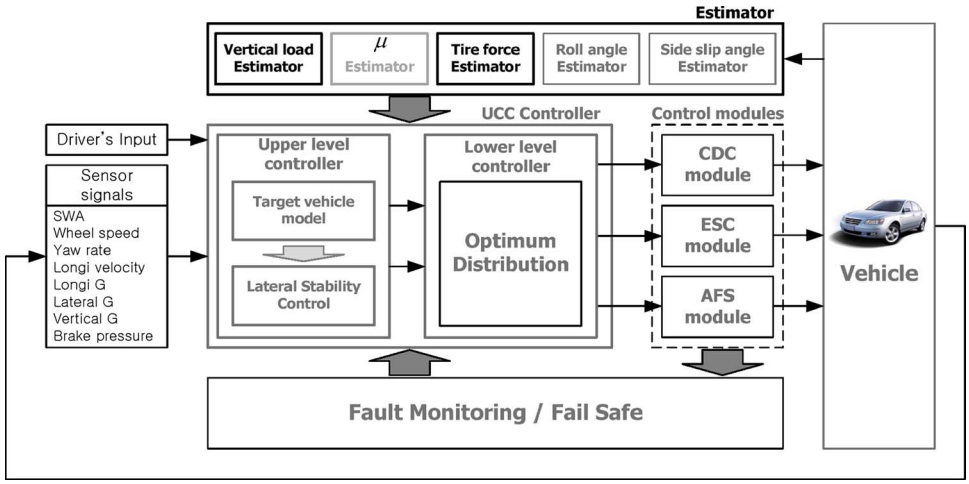

Fig. 1. Proposed UCC architecture.

$W_{LTR,R}$ Lateral load transfer of the rear-right wheel.
β Vehicle sideslip angle.
δ_f Tire steer angle.
γ Yaw rate.
γ_d Desired yaw rate.
ν_{couple} Coupling speed ratio of the torque converter $= 0.85$.

I. Introduction

TO IMPROVE the handling performance and the safety of vehicles, a considerable number of active control systems for the vehicle lateral dynamics have commercially been developed and utilized over the last two decades. Electronic stability control (ESC), which is the most popular system of all, has been well recognized to significantly improve vehicle lateral stability. In the case of the conventional ESC, the desired yaw moment is generated by differential braking. The deceleration of the vehicle, due to differential braking for yaw stability control, has a negative effect on the conventional ESC. To solve this problem, recent studies have shown that, by integrating individual modular chassis control systems such as the ESC, active front steering (AFS) and continuous damping control (CDC) can be achieved [1]–[4]. For optimized tire usage, to achieve a target vehicle response, an optimum longitudinal and lateral tire-force distribution by four-wheel independent steering, driving, and braking has been proposed [1]. A vehicle dynamics integrated control algorithm, using an online nonlinear optimization method, is proposed for four-wheel-distributed steering and four-wheel-distributed traction/braking systems [2]. Furthermore, to minimize the use of braking, the optimized coordination of the AFS and ESC has been proposed in a previous paper [4]. The longitudinal/lateral tire forces and the tire–road friction coefficients provide important information on the computation of the optimized active longitudinal and lateral tire forces to be generated by the AFS and ESC modules. This is the motivation for this paper, and the method for the estimation of the longitudinal/lateral tire forces will be proposed in this paper.

Recently, many analytical and experimental studies on the estimation of the longitudinal/lateral tire force and the friction coefficient between the tire and the road have been performed. An extended Kalman filter (EKF) has been implemented to estimate the state and the longitudinal and lateral tire-force histories of a 9-DOF vehicle [5]. This estimation process shows good robustness properties, even in the face of abrupt changes in road conditions. Lateral tire forces, the sideslip angle, and tire–road friction have been estimated by an adaptive observer that uses a combination of a vehicle model and a tire-force model [6]. The parameter-based and effect-based friction prediction/monitoring methods, using optical sensors at the front end of the car and strain sensors vulcanized into the tread element of a tire, have been presented [7]. The developed EKF estimates vehicle motions and tire forces as state estimates from a noisy measurement set [8]. The algorithms for reliable estimation of the friction coefficient, at each individual wheel of the vehicle, have been developed [9]. An adaptive observer based on the tire–road friction estimation method was proposed by Liu and Peng [10]. A sliding-mode observer, which is based on a LuGre friction model, and a simple representation of the vehicle have been designed by the measurements of the wheel speed and the applied brake pressure [11]. Kiencke and Daiß [12] use additional sensors such as the acceleration sensors or the braking pressure sensors to estimate the road-friction coefficients. Their method is based on a one-wheel model, and it requires dynamic wheel loads and brake pressures, in addition to wheel speeds. Observer-based methods (an observer-based least-square method and an observer/filtered-regressor-based method) for tire–road friction estimation have been presented [13]. The vehicle's state and the road conditions have been estimated using an estimation algorithm, which is formulated on the basis of the interacting multiple-model algorithm [14].

This paper presents an estimation strategy to estimate the longitudinal/lateral tire forces, which gives important information for use in unified-chassis-control (UCC) architectures. Fig. 1 shows a suitable overall UCC architecture, which consists of two parts: an estimator and a UCC controller. For the implementation of the proposed UCC architecture, various vehicle

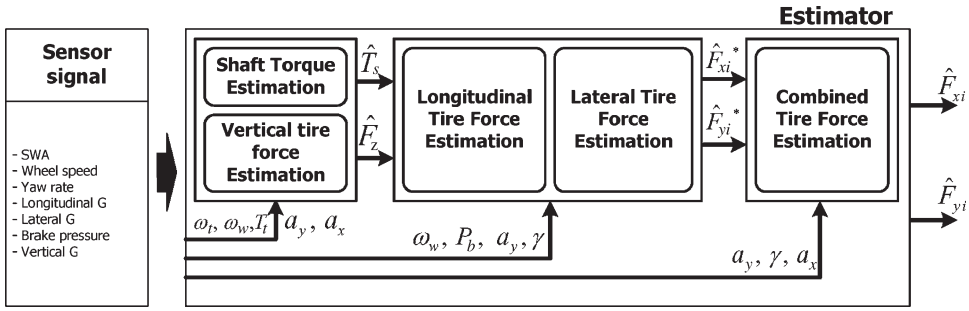

Fig. 2. Structure of the tire-force estimator.

parameters, such as the vehicle mass, its moment of inertia, the tire–road friction coefficient, tire cornering stiffness, etc., and the vehicle's state information, such as its sideslip angle, the longitudinal/lateral tire forces, the vertical tire forces, and the roll angle, are needed. However, these parameters and states are either very difficult or expensive to measure directly. A lot of research on the estimation of the vehicles' sideslip angle, roll angle, etc., has been conducted [15], [16], and the results have shown that the estimators can be designed using the available signals and can achieve good performance. In this paper, the estimator for the longitudinal/lateral tire forces has been designed. The longitudinal/lateral tire-force estimator consists of five steps, i.e., vertical tire-force estimation, shaft-torque estimation, longitudinal tire-force estimation, lateral tire-force estimation, and the combined tire-force estimation.

The performance of the proposed estimators has been evaluated via computer simulations conducted using the vehicle dynamic software CARSIM, the ASM vehicle model, and the estimators coded with Matlab/Simulink.

The rest of this paper is organized in the following manner. Section II describes the tire-force estimator. Section III presents the UCC system for the integration of a UCC controller and the estimator. Simulations for the evaluation of the UCC system are conducted, and conclusions are finally given in Section IV.

II. Tire-Force Estimator

In this section, the tire-force estimator is proposed for the estimation of the vertical, longitudinal, and lateral tire forces of each wheel. The estimator consists of the vertical tire-force estimation, the shaft torque estimation, the longitudinal tire-force estimation, the lateral tire-force estimation, and the combined tire-force estimation. The vertical tire force can simply be estimated by the longitudinal/lateral accelerations and roll states. This estimation scheme has been designed assuming that the roll state can be obtained by the use of a roll-state estimator designed in our previous study [16]. The shaft-torque estimator has been designed by using the turbine torque, the turbine angular velocity, and the wheel angular velocity. The longitudinal and lateral tire-force estimators can be estimated by the wheel angular velocity, the lateral acceleration, the longitudinal acceleration, and the yaw rate. The lateral acceleration, the longitudinal acceleration, and the yaw rate can easily be measured from already-existing sensors on the vehicle equipped with an ESC system. The combined tire-force estimator can be designed by using measurements such as longitudinal acceleration, lateral acceleration, and yaw rate.

These functions of the estimator will be explained in the following sections, and Fig. 2 shows the architecture of the proposed tire-force estimator that is developed in this paper. First, the vertical tire-force estimator and the shaft-torque estimator should be designed. Next, the longitudinal tire-force estimator is designed using the shaft torque, the vertical tire force, and the wheel angular velocity. Then, lateral tire force can be estimated by using longitudinal tire force, lateral acceleration, and yaw rate. Finally, the estimated longitudinal/lateral tire forces are compensated by the combined tire-force estimator.

A. Vertical Tire-Force Estimator

In the true vehicle model, the vertical tire force depends on the suspension dynamics, and it can be changed by the driver's maneuvers such as throttle, braking, and steering inputs or by road disturbances. Because of the complexity of the suspension dynamics and the difficulty in considering the road disturbance, many researchers have simply designed a vertical tire-force estimator considering only the driver's maneuvers, include no road disturbances and the suspension effect, and these have shown good performance for the estimator [5], [15]. These estimators have been designed by using the lateral and longitudinal accelerations. In this paper, the vertical tire-force estimator, which was summarized in previous research, will be introduced. This estimator is designed by using the lateral acceleration, longitudinal acceleration, and roll states.

The vertical tire forces $(F_{z,FL}, F_{z,FR}, F_{z,RL}, F_{z,RR})$ can be estimated by the summation of longitudinal load transfer W_{FA}, lateral load transfer $W_{LT^*,^*}$, and static normal force F_{SW^*}. The estimates of the vertical tire forces $\hat{F}_{zi}$ can be represented as follows:

$$\begin{aligned}
\hat{F}_{z,FL} &= \frac{1}{2}F_{SWF} - W_{LTF,L} - W_{FA} \\
\hat{F}_{z,FR} &= \frac{1}{2}F_{SWF} + W_{LTF,R} - W_{FA} \\
\hat{F}_{z,RL} &= \frac{1}{2}F_{SWR} - W_{LTR,L} + W_{FA} \\
\hat{F}_{z,RR} &= \frac{1}{2}F_{SWR} + W_{LTR,R} + W_{FA}.
\end{aligned} \tag{1}$$

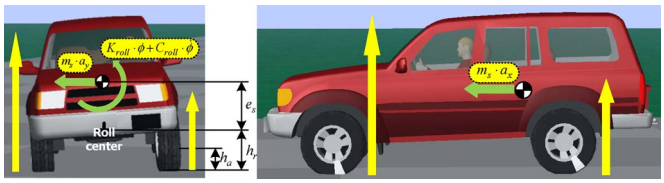

Fig. 3. Vehicle's roll model and longitudinal model.

Fig. 3 shows the vehicle's roll model and the longitudinal model. The sum of the lateral transfer $(W_{LTF} + W_{LTR})$ is determined from a 2-DOF vehicle roll model as follows:

$$W_{LTF} + W_{LTR} = \frac{(m_s h_r + m_u h_a)}{t} a_y + \frac{K_{\text{roll}}\phi + C_{\text{roll}}\dot{\phi}}{t} \tag{2}$$

where K_{roll} and C_{roll} are the combined roll damping coefficient and the combined roll stiffness coefficient, respectively.

The roll sate can be obtained by the use of a roll state estimator designed in our previous study [16]. Since the combined roll damping is largely due to the suspension damper and the damping rate of the damper significantly varies in the case of the CDC, using the following equality:

$$K_{\text{roll}}\phi + C_{\text{roll}}\dot{\phi} = m_s e_s (a_y - g\phi - e_s\ddot{\phi}) - I_{xxs}\ddot{\phi} \tag{3}$$

The lateral load transfer is estimated as follows:

$$W_{LTF} + W_{LTR} = \frac{(m_s h_r + m_u h_a)}{t} a_y + \frac{m_s e_s (a_y - g\phi - e_s\ddot{\phi}) - I_{xxs}\ddot{\phi}}{t}. \tag{4}$$

Equation (3) is obtained from an 8-DOF nonlinear vehicle model [17].

The longitudinal load transfer can be estimated using the vehicle's longitudinal acceleration

$$W_{FA} = \frac{m_s h_s}{2(l_f + l_r)} a_x. \tag{5}$$

To investigate the performance of the proposed vertical load estimator, simulations have been conducted without including any road disturbances. A sine-wave steering wheel angle with $\pm 60^\circ$ has been used at a deceleration situation. The vehicle initial speed was set to 80 km/h. The simulation results are shown in Fig. 4. Fig. 4(a) shows the longitudinal acceleration. Fig. 4(b)–(e) shows the front-left, front-right, rear-left, and rear-right vertical tire forces, respectively. According to the simulation results, the vertical tire-force estimator shows good performance on the road when there are no road disturbances.

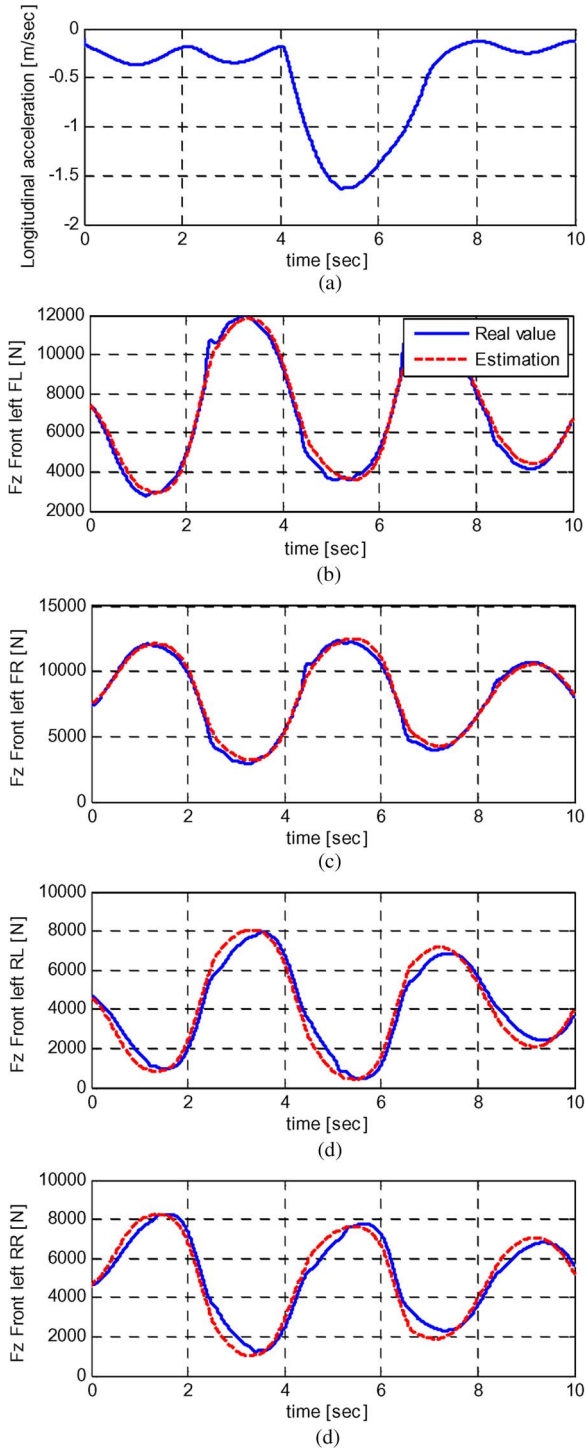

Fig. 4. Simulation results. Vertical load estimator. (a) Longitudinal acceleration. (b) Vertical tire force at the front-left tire. (c) Vertical tire force at the front-right tire. (d) Vertical tire force at the rear-left tire. (e) Vertical tire force at the rear-right tire.

B. Shaft Torque Estimation

A shaft torque can be estimated by using the turbine torque, the turbine angular velocity, and the wheel angular velocity [18], [20]. The turbine torque cannot be directly measured but can be determined by using the turbine angular velocity and the pump angular velocity as follows:

High-torque transfer phase $(\omega_t/\omega_p < \nu_{\text{couple}})$

$$T_t = c_1\omega_p^2 + c_2\omega_p\omega_t + c_3\omega_t^2. \tag{6}$$

Fluid couple mode $(\omega_t/\omega_p \geq \nu_{\text{couple}})$

$$T_t = c_4\omega_p^2 + c_5\omega_p\omega_t + c_6\omega_t^2. \tag{7}$$

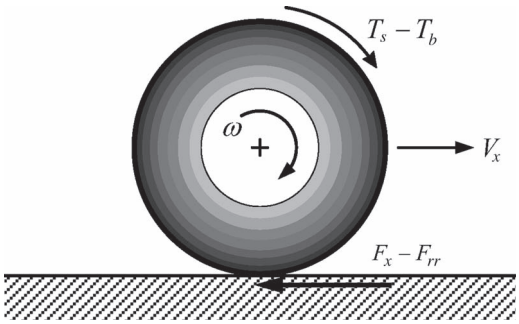

Fig. 5. Simplified wheel dynamics model.

The following equation shows the differential equation that estimates the shaft torque:

$$\dot{\omega}_t = \frac{T_t - T_s R_d R_i}{I_{cr}}$$
$$\dot{T}_s = K_s(R_d R_i \omega_t - \omega_w). \tag{8}$$

It is assumed that T_t, ω_t, and ω_w are available signals; hence, from (8), the state equation and the measurement equation are determined as follows:

$$\dot{x} = Ax + Bu + G \cdot w$$
$$z = Cx + v \tag{9}$$

where

$$A = \begin{bmatrix} 0 & -\frac{R_d R_i}{I_{cr}} \\ K_s R_d R_i & 0 \end{bmatrix} \quad B = \begin{bmatrix} \frac{1}{I_{cr}} & 0 \\ 0 & -K_s \end{bmatrix}$$
$$C = [1 \quad 0] \quad x = [\omega_t \quad T_s]^T \quad u = [T_t \quad \omega_w]^T.$$

Since the rank of the observability matrix about (9) is 2, the shaft torque can be estimated by using a Kalman filter

$$\hat{x} = A\hat{x} + Bu + L(z - C\hat{x}) \tag{10}$$

where L is the Kalman gain.

C. Longitudinal Tire-Force Estimation

The longitudinal tire force can be estimated by using the wheel's angular velocity, braking pressure, and shaft torque. This estimator is based on a simplified wheel dynamics model, which can be seen in Fig. 5.

The dynamics equation for Fig. 5 is given by

$$I_{\omega,i}\dot{\omega}_i = r_{w,i}F_{x,i} - T_{b,i} + T_s - r_{w,i}F_{rr} \tag{11}$$

where F_x, T_b, T_s, and $i = FL, FR, RL, RR$ are the longitudinal tire force, brake torque, shaft torque, and rolling resistance, respectively. It is assumed that the brake pressure of each wheel is the available signal. Therefore, the brake torque can be computed by the brake gain (K_{Bf}, K_{Br}). The shaft torque is the estimated value at the previous time instant, and the rolling resistance is the available signal. The effective radius of each wheel can also be determined by the vertical load, which is estimated in Section II

$$r_{w,i} = r - \frac{F_{z,i}}{K_t}. \tag{12}$$

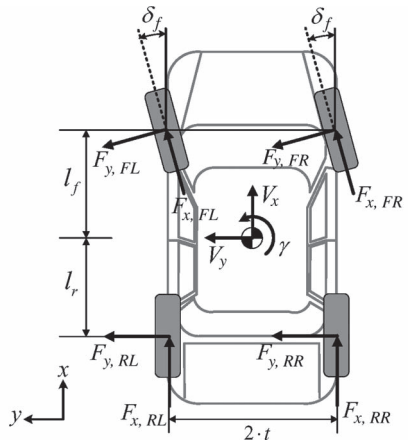

Fig. 6. Planar model.

The longitudinal tire force can be estimated by the wheel speed (ω) [9], and from (11), the wheel angular acceleration can be presented as follows:

$$\dot{\hat{\omega}}_i = \frac{1}{I_{\omega,i}}(r_{w,i}\hat{F}_{x,i} - T_{b,i} + T_s - r_{w,i}F_{rr}). \tag{13}$$

Define an energy function using the wheel's angular velocity V as

$$V = \frac{1}{2}(\omega_i - \hat{\omega}_i)^2. \tag{14}$$

Differentiating V gives

$$\dot{V} = (\dot{\omega}_i - \dot{\hat{\omega}}_i)(\omega_i - \hat{\omega}_i) \tag{15}$$

where ω_i is the wheel angular velocity from the wheel speed sensor, and $\hat{\omega}_i$ is the estimated wheel angular velocity. Substituting (13) into (15) yields

$$\dot{V} = \left(\dot{\omega}_i - \frac{r_{w,i}\hat{F}_{x,i} - T_{b,i} + T_s - r_{w,i}F_{rr}}{I_{\omega,i}}\right)(\omega_i - \hat{\omega}_i). \tag{16}$$

To satisfy the condition of the energy function $(\dot{V} = -\lambda_1(\omega_i - \hat{\omega}_i)^2)$, the estimated longitudinal tire force is determined as follows:

$$\hat{F}_{x,i} = \frac{1}{r_{w,i}}\left[I_{\omega,i}\left\{\dot{\omega}_i + \lambda_1(\omega_i - \hat{\omega}_i)\right\} + T_{b,i} - T_s + r_{w,i}F_{rr}\right]. \tag{17}$$

D. Lateral Tire-Force Estimation

The lateral tire-force estimator, which is based on the planar model, is designed by using the estimated longitudinal tire force, the lateral acceleration, and the yaw rate signal. Fig. 6 shows the planar model.

The lateral tire forces in Fig. 6 can be represented as follows:

$$\begin{aligned} F_{yf} &= F_{y,FL} + F_{y,FR} \\ F_{yr} &= F_{y,RL} + F_{y,RR}. \end{aligned} \tag{18}$$

For the small steering angle, the dynamic equations about the y-axis and yaw axis in the planar model can be presented as follows:

$$\begin{aligned} m(\dot{V}_y - \gamma V_x) &= ma_y \\ &= F_{yf} + F_{yr} + (\hat{F}_{x,FL} + \hat{F}_{x,FR})\delta_f \qquad (19) \\ I_Z\dot{\gamma} &= l_f F_{yf} - l_r F_{yr} \\ &\quad + t(-\hat{F}_{x,FL} + \hat{F}_{x,FR} - \hat{F}_{x,RL} + \hat{F}_{x,RR}) \\ &\quad + l_f(\hat{F}_{x,FL} + \hat{F}_{x,FR}) \cdot \delta_f. \qquad (20) \end{aligned}$$

The longitudinal tire forces of each wheel are the estimated values obtained from the longitudinal tire-force estimator. From (19) and (20), the estimated lateral tire forces can be calculated as follows:

$$\hat{F}_{yf} = \frac{ml_r a_y + I_Z\dot{\gamma} - t(\hat{F}_{x,FL} + \hat{F}_{x,RL} - \hat{F}_{x,FR} - \hat{F}_{x,RR}) - (l_f + l_r)(\hat{F}_{x,FL} + \hat{F}_{x,FR})\delta_f}{l_f + l_r} \tag{21}$$

$$\hat{F}_{yr} = \frac{ml_f a_y - I_Z\dot{\gamma} + t(\hat{F}_{x,FL} + \hat{F}_{x,RL} - \hat{F}_{x,FR} - \hat{F}_{x,RR})}{l_f + l_r}. \tag{22}$$

E. Combined Tire-Force Estimation

In the case of a normal driving situation, the estimators designed at the previous time instant show good performance. However, in extreme maneuvering cases, where the slip ratios are large, the performance of the estimator is not satisfactory, since the longitudinal tire-force estimator does not consider a slip ratio. To solve this problem, the random-walk Kalman filter is designed by using measurements such as longitudinal acceleration, lateral acceleration, and yaw rate and is based on the planar model in the combined tire-force estimator. To design the Kalman filter, new states are defined as follows:

$$\begin{aligned} &\xi_1 = F_{yf} - \hat{F}_{yf}, \qquad \xi_2 = F_{yr} - \hat{F}_{yr} \\ &\xi_3 = F_{x,FL} - \hat{F}_{x,FL}, \quad \xi_4 = F_{x,FR} - \hat{F}_{x,FR} \\ &\xi_5 = F_{x,RL} - \hat{F}_{x,RL}, \quad \xi_6 = F_{x,RR} - \hat{F}_{x,RR} \\ &x = [\,\xi_1 \quad \xi_2 \quad \xi_3 \quad \xi_4 \quad \xi_5 \quad \xi_6\,] \end{aligned} \tag{23}$$

where F_{yf}, F_{yr}, and $F_{x,i}$ are the real values, and $\hat{F}_{yf}$, $\hat{F}_{yr}$, and $\hat{F}_{x,i}$ $(i = FL, FR, RL, RR)$ are the estimated values at the previous time instant. Since the new defined states are random signals, these signals have no dynamics, as follows:

$$\dot{x} = w \tag{24}$$

where w is the process noise. The dynamic equations about the longitudinal and lateral accelerations and the yaw rate can be represented as follows:

$$\begin{aligned} ma_x &= F_{x,FL} + F_{x,FR} + F_{x,RL} + F_{x,RR} \\ &\quad - F_{yf} \cdot \delta_f - F_{x,\mathrm{aero}} \\ ma_y &= F_{yf} + F_{yr} + F_{x,FL} \cdot \delta_f + F_{x,FR}\delta_f \\ I_Z\dot{\gamma} &= l_f F_{yf} - l_r F_{yr} \\ &\quad + t(-F_{x,FL} + F_{x,FR} - F_{x,RL} + F_{x,RR}) \\ &\quad + l_f(F_{x,FL} + F_{x,FR})\delta_f. \end{aligned} \tag{25}$$

Equation (25) is from the planar model presented in Fig. 6. From the new states defined in (23) and (25), the measurement equation can be reformed as in (26), shown at the bottom of the page, where v is the measurement noise. Equation (26) can be expressed in measurement equation form as follows:

$$z = \begin{bmatrix} -\delta_f & 0 & 1 & 1 & 1 & 1 \\ 1 & 1 & \delta_f & \delta_f & 0 & 0 \\ l_f & -l_f & -t + l_f\delta_f & t + l_f\delta_f & -t & t \end{bmatrix} x + v. \tag{27}$$

From (24) and (27), the state equation in this estimator is presented as follows:

$$\begin{aligned} \dot{x}(t) &= w(t) \\ z(t) &= Hx(t) + v(t). \end{aligned} \tag{28}$$

Equation (28) can be changed to a discrete form as follows:

$$\begin{aligned} x_{k+1} &= A_k x_k + w_k \\ z_k &= H_k x_k + v_k \end{aligned} \tag{29}$$

where

$$A_k = e^{[0]T} = I \quad w_k = \int_{k\cdot T}^{(k+1)T} w(\tau)\, d\tau$$

$$H_k = H \quad v_k = v \quad T : \text{Time interval.}$$

$$\begin{aligned} z &= \begin{bmatrix} ma_x - \hat{F}_{x,FL} - \hat{F}_{x,FR} - \hat{F}_{x,RL} - \hat{F}_{x,RR} + \hat{F}_{yf}\delta_f + F_{x,aero} \\ ma_y - \hat{F}_{yf} - \hat{F}_{yr} - (\hat{F}_{x,FL} + \hat{F}_{x,FR}) \cdot \delta_f \\ I_Z\dot{\gamma} - l_f\hat{F}_{yf} + l_r\hat{F}_{yr} + t(\hat{F}_{x,FL} - \hat{F}_{x,FR}\hat{F}_{x,RL} - \hat{F}_{x,RR}) \\ -l_f(F_{x,FL} + F_{x,FR})\delta_f \end{bmatrix} + v \\ &= \begin{bmatrix} -\delta_f \cdot \xi_1 + \xi_3 + \xi_4 + \xi_5 + \xi_6 \\ \xi_1 + \xi_2 + \delta_f(\xi_3 + \xi_4) \\ l_f\xi_1 - l_r\xi_2 + t(-\xi_3 + \xi_4 - \xi_5 + \xi_6) + l_f\delta_f(\xi_3 + \xi_4) \end{bmatrix} + v \end{aligned} \tag{26}$$

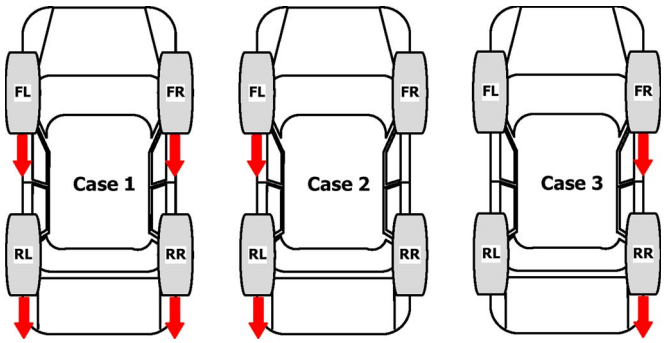

Fig. 7. Cases of the estimator.

The estimator consists of two steps, namely, the measurement update step and the time update step. The details of these are given as follows:

Measurement update

$$\hat{x}_k = \overline{x}_k + K_k[z_k - H_k\overline{x}_k] \tag{30}$$

where

$$\begin{cases} K_k = P_k H_k^T V_k^{-1} \\ P_k^{-1} = M_k^{-1} + H_k^T V_k^T H_k. \end{cases}$$

Time update

$$\begin{aligned} \overline{x}_{k+1} &= \hat{x}_k \\ M_{k+1} &= P_k + W_k. \end{aligned} \tag{31}$$

To calculate the Kalman gain (K_k) in the measurement update step, a 6×6 inverse matrix of the error covariance (P_k) should be computed. In this case, because of the computation load, it is hard to apply in a real-time implementation. To solve this problem, the inverse matrix of the error covariance has been changed into a 3×3 inverse matrix by using the inverse matrix formula as follows:

$$P_k = M_k - M_k H_k^T \left[H_k M_k H_k^T + V_k^{T-1}\right]^{-1} H_k M_k. \tag{32}$$

The random-walk Kalman filter estimates random signals depending only on the measurements. In the case of a small number of states and when a large number of measurements are available, the estimator performs well. Since the number of measurements is specified, the state reduction is accomplished to design the estimator corresponding to some specific cases. In the case of differential braking for the ESC, the tire, without braking, seems to be in the small-slip-ratio region. Therefore, in the case of the tire in the small-slip-ratio region, the longitudinal tire forces, which were estimated in Section III-B, are assumed to be the real values. Fig. 7 shows different cases of the estimator.

- Case 1 (Four-wheel braking or no braking)
  States: $x = [\xi_1 \quad \xi_2 \quad \xi_3 \quad \xi_4 \quad \xi_5 \quad \xi_6]^T$.
- Case 2 (Left-wheel braking)
  States: $x = [\xi_1 \quad \xi_2 \quad \xi_3 \quad \not{\xi}_4 \quad \xi_5 \quad \not{\xi}_6]^T$.
- Case 3 (Right-wheel braking)
  States: $x = [\xi_1 \quad \xi_2 \quad \not{\xi}_3 \quad \xi_4 \quad \not{\xi}_5 \quad \xi_6]^T$.

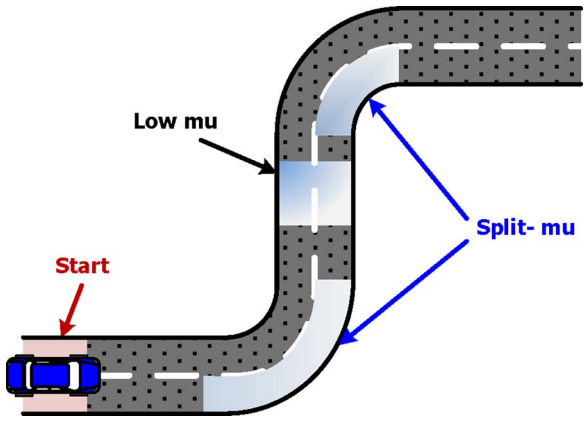

Fig. 8. Reference trajectory of the vehicle.

F. Simulation Results

The proposed tire-force estimator was evaluated through the computer simulations using CARSIM, the ASM vehicle model, and Matlab/Simulink. CARSIM and the ASM vehicle model are vehicle simulation software, and the tire-force estimator is implemented within the Matlab/Simulink environment. To show the good performance of the estimator, irrespective of the vehicle model, two vehicle models were used in the simulations. In addition, two simulations were conducted to test the performance of the estimator. One was a simulation to track a reference trajectory with various values of the tire–road friction coefficient, and the other was an open-loop steering simulation for single-lane changes.

1) Simulation Results Using Closed-Loop Driver–Vehicle–Controller System: A combined steering, throttle, and braking maneuver for tracking the reference trajectory is simulated on a road surface with various tire–road friction coefficient values. This simulation is based on the ASM vehicle model. A wheel steering angle, throttle angle, and braking pressure are determined by a human driver model, which is included in the ASM vehicle model. Fig. 8 shows the reference trajectory of the vehicle.

The tire-force estimates are presented in Fig. 9. The tire–road friction coefficient changes from 1 to 0.3. The velocity profile of the vehicle is shown in Fig. 9(a), and Fig. 9(b)–(g) shows the front-left longitudinal tire force, the front-right longitudinal tire force, the rear-left longitudinal tire force, the rear-right longitudinal tire force, the front lateral tire force, and the rear lateral tire force, respectively. During the time interval $t = 22 \sim 24$ of the simulation, the vehicle travels in a straight line and accelerates for low μ values (0.3). At $t = 28 \sim 30$, the vehicle turns and applies the brake on the second corner with a split-mu, and these are the reasons for the increasing slip ratio of the tire. Since the longitudinal tire-force estimation, which is designed in Sections II and III, does not consider the slip ratio, a large slip ratio can produce a negative effect for the longitudinal tire-force estimator. From the simulation results, it is known that the longitudinal tire-force estimator results, prior to the combined tire-force estimator, are not good at $t = 22 \sim 24$ s and $t = 28 \sim 30$ s. On the other hand, the results of the proposed estimator in this paper are very good,

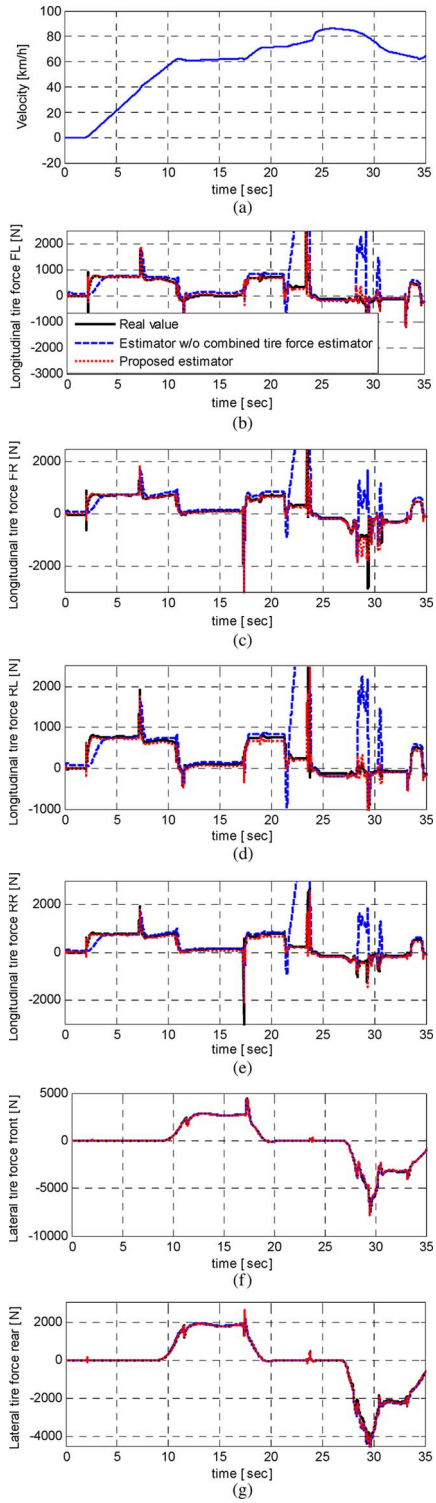

Fig. 9. Simulation results from using a human driver model. (a) Velocity profile. (b) Front-left longitudinal tire force. (c) Front-right longitudinal tire force. (d) Rear-left longitudinal tire force. (e) Rear-right longitudinal tire force. (f) Front lateral tire force. (g) Rear lateral tire force.

even though the change in the tire–road friction coefficient is unknown to the estimator.

2) Simulation Results Using Open-Loop Single-Lane Change Maneuver: The simulation results mentioned in the previous section do not consider the sensor noise. To investigate the performance of the estimator, with respect to the sensor noise, an open-loop single-lane-change maneuver simulation, considering the sensor noise, was performed for the vehicle driving on the split-μ (0.3 versus 0.85) with an initial forward speed of 80 km/h. Since the acceleration sensors are most affected by noises, in this simulation case, the sensor noise during the lateral and longitudinal accelerations has been added to the signals. The mean and error covariance values of the signals can be determined based on the test data and are represented as follows:

$$\begin{aligned} a_{x,\text{sensor}} &= a_x + n_x \\ a_{y,\text{sensor}} &= a_y + n_y \end{aligned} \tag{33}$$

where

$$\begin{aligned} n_x &\sim N\left(0, \sigma_x^2\right) \quad n_y \sim N\left(0, \sigma_y^2\right) \\ \sigma_x &= 0.01 \text{ m/s}^2 \quad \sigma_y = 0.01 \text{ m/s}^2. \end{aligned}$$

The conventional ESC was used for the improvement of the vehicle lateral stability. Furthermore, to evaluate the performance of the tire-force estimator in a critical driving situation (wheel-locking situation), the antilock braking system was not used. This means that the differential braking of the ESC can be one reason that the wheel locked.

Fig. 10(a) shows the time histories of the steering angle, and Fig. 10(b) shows the brake pressures of each wheel from the ESC. Fig. 10(c) and (d) shows the front-left longitudinal and front lateral tire forces, respectively. As shown in Fig. 10(e), wheel locking at the front-left and rear-left tire occurs at around 7–9 s. From the simulation results, it is found that the tire-force estimator, which includes the sensor noise, also performed well, even in the wheel-locking situation.

III. Simulation Study of the Estimator Performance of a UCC System

In this section, the UCC system, including the UCC controller and the estimator, will be described. Since the estimator has already been described in the previous section, the UCC controller is introduced here. It should be noted that this paper does not focus on the vehicle stability control; therefore, the UCC controller is introduced only to give a case application of the estimator. In this context, the details of the UCC controller are not presented in this paper. The proposed UCC system for maneuverability and lateral stability was evaluated through the computer simulations using the vehicle-simulation softwares CARSIM and Matlab/Simulink.

A. UCC Controller

This section presents the UCC controller, which is generally used to improve vehicle lateral stability. The UCC controller has been designed in two stages, namely, the upper and lower level stages. The upper level controller is based on the driver's steering input to determine the target response for the vehicle, as well as the desired yaw moment based on the yaw motions. The desired yaw moment, which is based on a 2-D bicycle model, is designed by a sliding-mode control (SMC) considering tire cornering stiffness uncertainties. In the case of the

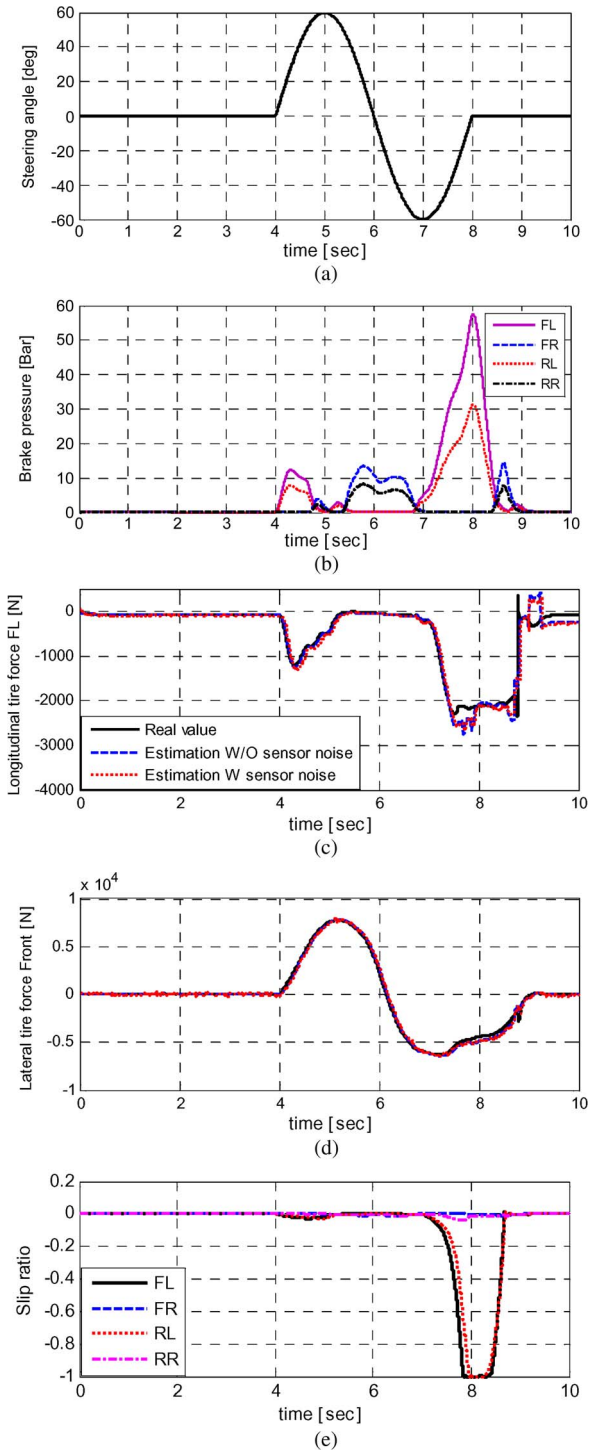

Fig. 10. Simulation results of the open-loop single lane change @ 80 km/hr. (a) Steering wheel angle. (b) Braking pressure. (c) Front-left longitudinal tire force. (d) Front lateral tire force. (e) Slip ratio.

conventional ESC, the desired yaw moment is generated by the differential braking. This can lead to longitudinal decelerations that are not intended by the driver. These can also lead to a loss of ride comfort. Additionally, the brake control input can lead to wear on the tires and the brakes. To solve this problem, the lower level controller computes the active longitudinal/lateral tire forces for the desired yaw moment to minimize the longitudinal deceleration. The integrated optimum control law is designed by using the Karush–Kuhn–Tucker condition [4].

In this controller, a target vehicle dynamic response γ_d for a driver's steering input δ_f is defined as follows:

$$\gamma_d = \frac{\gamma_{ss}}{1+\tau_e s}\delta_f \tag{34}$$

where τ_e is the Time constant

$$\gamma_{ss} = \frac{2V_x C_f C_r (l_f + l_r)}{2C_f C_r (l_f + l_r)^2 - mV_x^2 (l_f C_f - l_r C_r)}.$$

At the high-level controller, since the tire cornering stiffness has inherent nonlinearity and uncertainty, the SMC method has been used for the design of the desired yaw moment to directly incorporate the uncertainties into the control design stage.

$$\Delta M_Z = M_{Z,eq} - k_1 sat\left(\frac{\gamma-\gamma_d}{\Phi_1}\right) \tag{35}$$

represents the desired yaw moment, where

$$M_{Z,eq} = -I_Z\left(\frac{2(-l_f\hat{C}_f + l_r\hat{C}_r)}{I_Z}\beta - \frac{2\left(l_f^2\hat{C}_f + l_r^2\hat{C}_r\right)}{I_Z V_x}\gamma + \frac{2l_f\hat{C}_f}{I_Z}\delta_f\right)$$

$$k_1 = I_Z\left\{F_f\left|-\frac{l_f}{I_Z}\beta - \frac{l_f^2}{I_Z}\gamma + \frac{l_f}{I_Z}\delta_f\right| + F_r\left|\frac{l_r}{I_Z}\beta - \frac{l_r^2}{I_Z}\gamma\right| + |\dot{\gamma}_d| + \eta_1\right\}.$$

At the lower level controller, an optimized coordination of the active longitudinal and lateral tire forces has been used to minimize the usage of braking. The solution of the optimization process is changed by the sign of the desired yaw moment. In the case of the positive desired yaw moment, the solution at the front-left tire is determined as follows:

$$\text{i)} \quad \Delta M_Z \geq 0. \tag{36}$$

$$\text{Case 1}: \Delta F_{x,FL} = 0 \quad \Delta F_{y,FL} = \frac{\Delta M_Z}{l_f D_2}$$

$$\text{Case 2}: \Delta F_{x,FL} = \frac{-(F_{x,FL}+\kappa\zeta) + \sqrt{(1+\kappa^2)\mu^2 F_{z,FL}^2 - (\kappa F_{z,FL} - \zeta)^2}}{(1+\kappa^2)}$$

$$\Delta F_{y,FL} = \frac{tD_1}{2l_f D_2}\Delta F_{x,FL} + \frac{1}{l_f D_2}\Delta M_Z$$

where

$$D_1 = 1 + \frac{F_{z,RL}}{F_{z,FR}} \quad D_2 = 1 + \frac{F_{z,FR}}{F_{z,FL}}$$

$$\kappa = \frac{tD_1}{2l_f D_2} \quad \zeta = \frac{1}{l_f D_2}\Delta M_Z + F_{y,FL}.$$

In Case 1, it is implied that the sum of each lateral and longitudinal tire force is smaller than the friction of the tire. On the other hand, in Case 2, it is implied that the sum of each lateral and longitudinal tire force is equal to the friction of the

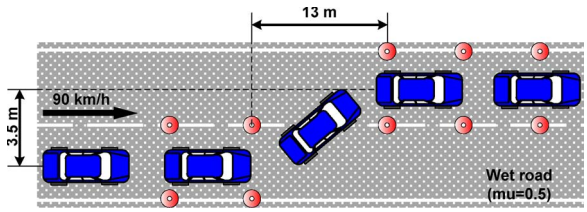

Fig. 11. Reference trajectory of the vehicle for the single-lane change maneuver.

tire. In the case of a negative desired yaw moment, the active lateral and longitudinal tire forces can be obtained as follows:

ii) $\Delta M_Z < 0.$ (37)

Case 1: $\Delta F_{x,FR} = 0 \quad \Delta F_{y,FR} = \dfrac{\Delta M_Z}{l_f E_2}$

Case 2: $\Delta F_{x,FR}$

$$= \frac{-(F_{x,FR}+\kappa\zeta)+\sqrt{(1+\kappa^2)\mu^2 F_{z,FR}^2-(\kappa F_{z,FR}-\zeta)^2}}{(1+\kappa^2)}$$

$$\Delta F_{y,FR} = -\frac{tE_1}{2l_f E_2}\Delta F_{x,FR} + \frac{1}{l_f E_2}\Delta M_Z$$

where

$$E_1 = 1+\frac{F_{z,RR}}{F_{z,FR}} \quad E_2 = 1+\frac{F_{z,FL}}{F_{z,FR}}$$

$$\kappa = \frac{tE_1}{2l_f E_2} \quad \zeta = \frac{1}{l_f E_2}\Delta M_Z + F_{y,FR}.$$

B. Simulation Results

The proposed UCC controller, including the estimator, was evaluated through the computer simulations. A single-lane change maneuver has been simulated on a wet road ($\mu = 0.5$). The initial speed was set to be 90 km/h, and a constant throttle input has been applied during the simulation study. In this paper, the wheel steering angle is determined by a human driver model, which is developed to represent the steering behavior of a human driver using a finite-preview optimal-control method [19]. It is designed to minimize a performance index defined as a quadratic form of the lateral position error, yaw angle error, and steering input. A neuromuscular system of a human driver is investigated using laboratory tests and is included in the development of the human driver steering model. For the general driving situation, the simulations are conducted at an arbitrary road profile, and Fig. 11 shows a reference trajectory of the vehicle.

Fig. 12 shows the simulation results of the proposed estimator, and Fig. 12(a) and (b) shows the front-left and front-right longitudinal tire forces, respectively. Fig. 12(c) and (d) shows the front and rear lateral tire forces. As shown in Fig. 12(a)–(d), the proposed tire-force estimator shows good performance.

Furthermore, the simulations to evaluate the performance of the controller using the tire-force estimator have been conducted. Fig. 13 shows the simulation results to investigate the performance of the UCC controller with the proposed estimator. Fig. 13(a) shows the steering wheel angle using the human driver model [20]. In the case of no control, since the vehicle runs off the track, it can be shown that the steering-wheel angle of the driver is increased more and more. The yaw rate error, sideslip angle, and longitudinal velocity of the vehicle that is not controlled and that controlled by the UCC system are shown in Fig. 13(b)–(d), respectively. Fig. 13(e) and (f) shows the control inputs of the AFS and ESC. From the simulation results, the UCC controller with the proposed estimator performs well in terms of yaw rate, sideslip angle, and path-tracking performance. Furthermore, it can be seen from Fig. 13(d) that the objective of the UCC controller, which minimizes longitudinal deceleration, is satisfied. These results demonstrate that the proposed estimators are effective in the UCC controller.

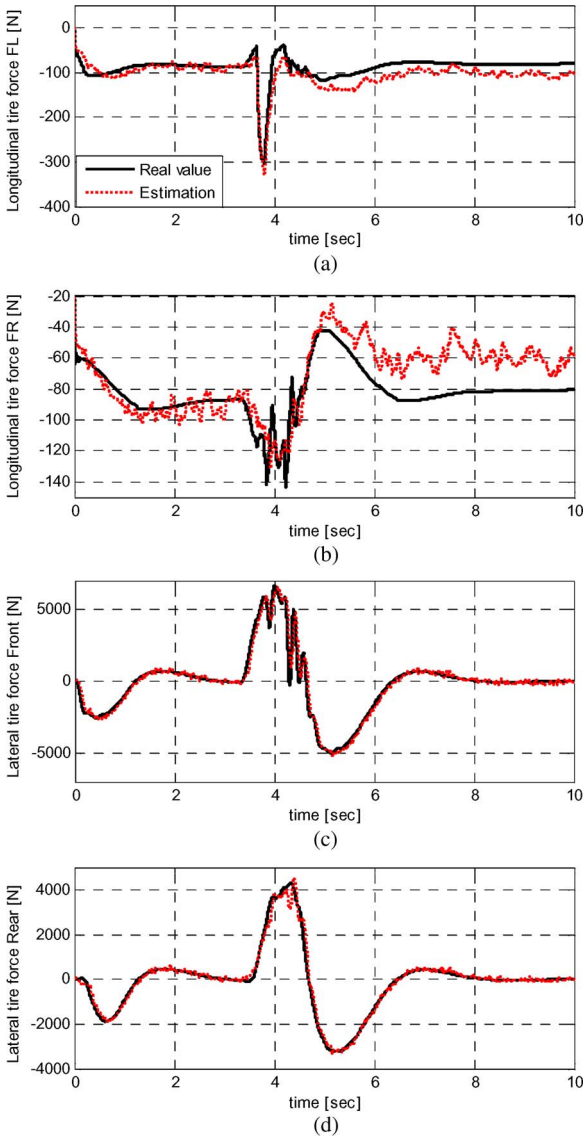

Fig. 12. Simulations results of the estimator. (a) Front-left longitudinal tire force. (b) Front-right longitudinal tire force. (c) Front lateral tire force. (d) Rear lateral tire force.

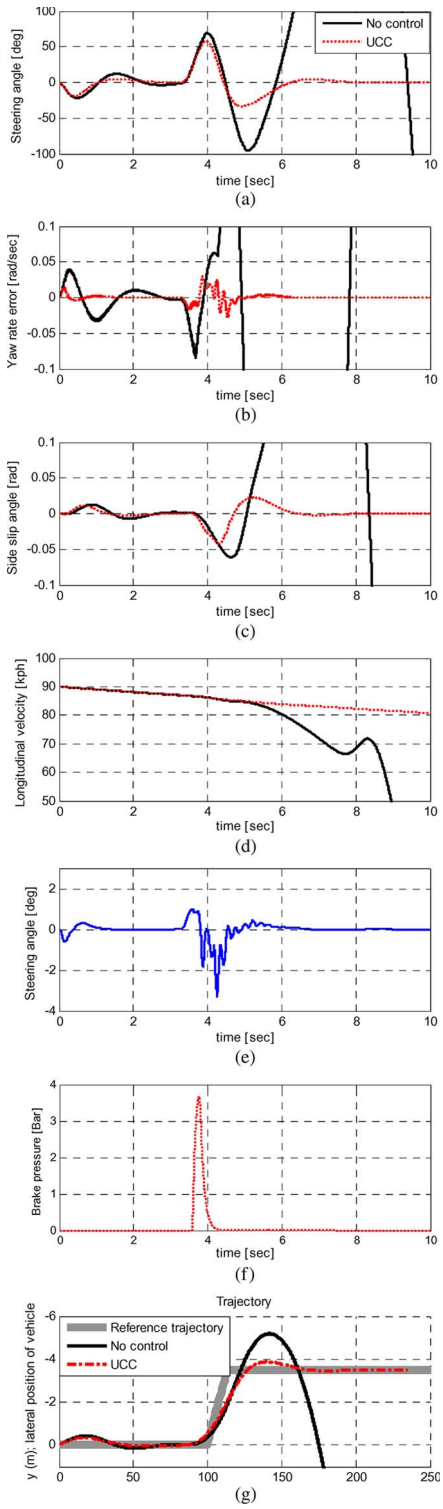

Fig. 13. Simulation results of the vehicle's responses and control inputs. (a) Steering wheel angle. (b) Yaw rate error. (c) Sideslip angle. (d) Longitudinal velocity. (e) Active steering of the front wheel. (f) Braking pressure at the front-left tire. (g) Trajectory.

IV. Conclusion

An estimation method for the determination of tire forces, for application to vehicle stability control, has been proposed. The tire-force estimator consists of five steps: 1) vertical tire-force estimation; 2) shaft torque estimation; 3) longitudinal tire-force estimation; 4) lateral tire-force estimation; and 5) combined tire-force estimation. From the simulation results, it is confirmed that the tire-force estimator performs well under various driving situations. Random road excitations and sensor noise conditions have also been considered in the simulation studies.

The proposed estimator has been used for the implementation of a stability control algorithm on a vehicle, i.e., a UCC algorithm. The performance of the UCC controller with the estimators has been investigated via closed-loop driver–vehicle–controller computer simulations. The simulated results have shown that the UCC algorithm can be successfully implemented with the estimated tire forces.

References

[1] O. Mokhiamar and M. Abe, "Simultaneous optimal distribution of lateral and longitudinal tire forces for the model following control," *Trans. ASME J. Dyn. Syst. Meas. Control*, vol. 126, no. 4, pp. 753–762, Dec. 2004.

[2] E. Ono, Y. Hattori, Y. Muragishi, and K. Koibuchi, "Vehicle dynamics integrated control for four-wheel-distributed steering and four-wheel-distributed traction/braking systems," *Veh. Syst. Dyn.*, vol. 44, no. 2, pp. 139–151, Feb. 2006.

[3] J. Wang and R. G. Longoria, "Coordinated vehicle dynamics control with control distribution," in *Proc. Amer. Control Conf.*, 2006, pp. 5348–5353.

[4] W. Cho, J. Yoon, J. Kim, J. Hur, and K. Yi, "An investigation into unified chassis control scheme for optimized vehicle stability and maneuverability," *Veh. Syst. Dyn.*, vol. 46, no. 1, pp. 87–105, 2008.

[5] L. R. Ray, "Nonlinear tyre force estimation and road friction identification: Simulation and experiments," *Automatica*, vol. 33, no. 10, pp. 1819–1833, Oct. 1997.

[6] G. Baffet, A. Charara, and G. Dherbomez, "An observer of tire-road forces and friction for active security vehicle systems," *IEEE/ASME Trans. Mechatron.*, vol. 12, no. 6, pp. 651–661, Dec. 2007.

[7] U. Eichhorn and J. Roth, "Prediction and monitoring of tyre/road friction," in *Proc. FISITA*, London, U.K., 1992, pp. 67–74.

[8] M. A. Wilkin, W. J. Manning, D. A. Crolla, and M. C. Levesley, "Estimation of non-linear friction force between tyre and road applied to a performance vehicle," in *Proc. AVEC*, 2004, pp. 387–392.

[9] R. Rajamani, D. Piyabongkarn, J. Y. Lew, and J. A. Grogg, "Algorithms for real-time estimation on individual wheel tire-road friction coefficients," in *Proc. Amer. Control Conf.*, 2006, pp. 4682–4687.

[10] C. Liu and H. Peng, "Tire-road friction estimation for the CAPC system," *Adv. Autom. Technol.*, vol. DSC-56/DE-86, pp. 71–77, 1995, Amer. Soc. Mech. Eng.

[11] N. Patel, C. Edwards, and S. K. Spurgeon, "A sliding mode observer for tyre friction estimation during braking," in *Proc. Amer. Control Conf.*, 2006, pp. 5867–5872.

[12] U. Kiencke and A. Daiß, "Estimation of tyre friction for enhanced ABS-systems," in *Proc. AVEC*, 1994, pp. 515–520.

[13] K. Yi, K. Hedrick, and S.-C. Lee, "Estimation of tire-road friction using observer based identifiers," *Veh. Syst. Dyn.*, vol. 31, no. 4, pp. 233–261, Apr. 1999.

[14] H. Tsunashima, M. Murakami, and J. Miyata, "Vehicle and road state estimation using interacting multiple model approach," *Veh. Syst. Dyn.*, vol. 44, pp. 750–758, 2006, Supplement.

[15] S.-H. You, S. Yoo, J.-O. Hahn, H. Lee, and K. I. Lee, "A new adaptive approach to real-time estimation of vehicle sideslip and road bank angle," in *Proc. Int. Symp. Adv. Veh. Control*, 2006, pp. 427–432.

[16] J. Yoon, J.-I. Park, K. Yi, and D. Kim, "Roll state estimator for application to rollover mitigation control," *Veh. Syst. Dyn.*, vol. 45, no. 5, pp. 459–475, 2007.

[17] S. Bae, J. R. Yun, J. M. Lee, and T. O. Tak, "An effect of the complexity in vehicle dynamics models on the analysis of vehicle dynamics behaviors: Model comparison and validation," *Korean Soc. Automotive Eng.*, vol. 8, no. 6, pp. 267–278, 2000.

[18] T. Jeong, K. Yi, and C. K. Song, "Estimation of tire-road friction coefficient using observers," *J. Control, Autom. Syst. Eng.*, vol. 4, no. 6, pp. 722–728, Feb. 1998.

[19] J. Kang, K. Yi, S. Yi, and K. Noh, "Development of a finite optimal preview control-based human driver steering model," in *Proc. Korean Soc. Automotive Eng., Spring Conf.*, 2006, vol. 3, pp. 1632–1637.

[20] R. A. Masmoudi and J. K. Hedrick, "Estimation of vehicle shaft torque using nonlinear observers," *Trans. ASME J. Dyn. Syst. Meas. Control*, vol. 114, no. 3, pp. 394–400, Sep. 1992.

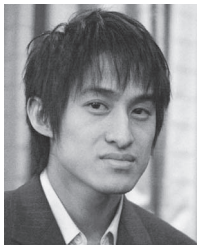

Wanki Cho received the B.S. degree in mechanical engineering in 2004 from Hanyang University, Seoul, Korea, and the M.S. degree in mechanical and aerospace engineering in 2006 from Seoul National University, where he is currently working toward the Ph.D. degree in mechanical and aerospace engineering with the School of Mechanical and Aerospace Engineering.

His research interest is the unified chassis control of a vehicle.

Jangyeol Yoon received the B.S. and M.S. degrees in mechanical engineering and mechanical design engineering from Hanyang University, Seoul, Korea, in 2003 and 2005, respectively. He is currently working toward the Ph.D. degree in mechanical and aerospace engineering with the School of Mechanical and Aerospace Engineering, Seoul National University.

His research interests are the lateral stability and rollover prevention control of a vehicle.

Seongjin Yim received the B.S. degree in mechanical engineering from Yonsei University, Seoul, Korea, in 1995 and the M.S. and Ph.D. degrees in mechanical engineering from the Korea Advanced Institute of Science and Technology, Daejeon, Korea, in 1997 and 2007, respectively.

Since 2008, he has been a Postdoctoral Researcher with the BK21 School for Creative Engineering Design of Next Generation Mechanical and Aerospace System, Seoul National University. His research interests are robust control, vehicle rollover prevention, and unified chassis control systems.

Bongyeong Koo received the academic degree in electronics from Gyeongsang National University, Jinju, Korea, in 1991.

Currently, he is a Senior Research Engineer with the Central R&D Center, Mando Corporation, Kyonggi-Do, Korea. His research interests are chassis control systems, active safety systems, and the integrated chassis control system of a ground vehicle.

Kyongsu Yi received the B.S. and M.S. degrees in mechanical engineering from Seoul National University, Seoul, Korea, in 1985 and 1987, respectively, and the Ph.D. degree in mechanical engineering from the University of California, Berkeley, in 1992.

From 1993 to 2005, he was with the School of Mechanical Engineering, Hanyang University, Seoul. Currently, he is a Professor with the School of Mechanical and Aerospace Engineering, Seoul National University. He currently serves as a member of the editorial boards of the *International Journal of Automotive Technology* and the Korean Society of Mechanical Engineers (KSME) and Institute of Control, Robotics and Systems journals. He is currently the Director of Vehicle Dynamics and Control Laboratory. His research interests are control systems, driver-assistance systems, and active safety systems of a ground vehicle.

Dr. Yi is a member of the American Society of Mechanical Engineers, the KSME, the Society of Automotive Engineers, and the Korean Society of Automotive Engineers (KSAE). He received the PAEKAM Paper Award from the KSME in 1997 and the Academic Award from the KSAE in 2004.